Cytosolic delivery of nano-labels prevents their asymmetric inheritance and enables extended quantitative *in vivo* cell imaging

Ranhua Xiong[1,2], Freya Joris[1], Sayuan Liang[3], Riet De Rycke[4,5], Saskia Lippens[4,5], Jo Demeester[1], Andre Skirtach[6,7], Koen Raemdonck[1], Uwe Himmelreich[3], Stefaan C. De Smedt[1], Kevin Braeckmans[1,2,8,9*]

[1]Laboratory of General Biochemistry and Physical Pharmacy, Ghent University, 9000 Ghent, Belgium

[2]Centre for Nano- and Biophotonics, Ghent University, 9000 Ghent, Belgium

[3]Biomedical NMR Unit, Faculty of Medicine, Katholieke Universiteit Leuven, 3000 Leuven, Belgium

[4]Inflammation Research Center, Image Core Facility, VIB, 9052 Ghent, Belgium;

[5]Department of Biomedical Molecular Biology, Ghent University, 9052 Ghent, Belgium.

[6]Department of Molecular Biotechnology, Ghent University, 9000 Ghent, Belgium

[7]Max-Planck Institute of Colloids and Interfaces, 14424 Potsdam, Germany

[8]Univ Lille 1, Univ Lille Nord France, IEMN, UMR 8520, 59652 Villeneuve Dascq, France

[9]Univ Lille 1, Univ Lille Nord France, Lab Phys Lasers Atomes & Mol, UMR 8523, 59655 Villeneuve Dascq, France

***Email: Kevin.Braeckmans@UGent.be**

Abstract

Long-term *in vivo* imaging of cells is crucial for the understanding of cellular fate in biological processes in cancer research, immunology or in cell-based therapies such as beta cell transplantation in type I diabetes or stem cell therapy. Traditionally, cell labelling with the desired contrast agent occurs *ex vivo via* spontaneous endocytosis, which is a variable and slow process that requires optimization for each particular label-cell type combination. Following endocytic uptake, the contrast agents mostly remain entrapped in the endolysosomal compartment, which leads to signal instability, cytotoxicity and asymmetric inheritance of the labels upon cell division. Here, we demonstrate that these disadvantages can be circumvented by delivering contrast agents directly into the cytoplasm *via* vapour nanobubble photoporation. Compared to classic endocytic uptake, photoporation resulted in 50 and 3 times higher loading of fluorescent dextrans and quantum dots, respectively, with improved signal stability and reduced cytotoxicity. Most interestingly, cytosolic delivery by photoporation prevented asymmetric inheritance of labels by daughter cells over subsequent cell generations. Instead, unequal inheritance of endocytosed labels resulted in a dramatic increase in polydispersity of the amount of labels per cell with each cell division, hindering accurate quantification of cell numbers *in vivo* over time. The combined benefits of cell labelling by photoporation resulted in a marked improvement in long-term cell visibility *in vivo* where an insulin producing cell line (INS-1E cell line) labelled with fluorescent dextrans could be tracked for up to two months in Swiss Nude mice compared to two weeks for cells labelled by endocytosis.

Keywords: *cell labelling, cytosolic delivery, nanoparticle inheritance, vapour nanobubble photoporation, in vivo cell tracking, quantum dots*

Introduction

There is great interest in monitoring *in vivo* transplanted cells for research and therapeutic purposes. In cancer research, for instance, it is of importance to visualize cancer cells in real time to study their metastatic potential in animal models[1]. *In vivo* tracking of cells is also desired for cell therapies to follow-up on treatment efficacy[2]. Examples are stem cells in regenerative medicine[3, 4], β-cells for the treatment of type I diabetes[5] and immune cells such as T-cells in immunotherapy[6].

For *in vivo* cell tracking, the cells need to be labelled before transplantation, for which two main strategies are being explored. One is to transfect the cells with a reporter gene[2, 7] and follow-up on their proliferation through optical imaging, positron emission tomography or magnetic resonance imaging[8-10]. This strategy, however, requires a rather time-consuming transfection procedure that may lead to undesired phenotypical alterations and abnormalities in the transplanted cells in comparison to the native cells[11-13]. The second strategy is to label the cells with exogenous contrast agents, being either organic probes or inorganic nanoparticles (NPs)[14, 15]. Examples are fluorescently labelled dextrans[16, 17] and quantum dots (QD) for optical fluorescence imaging[18-20], or superparamagnetic iron oxide NPs and Gadolinium complexes for magnetic resonance imaging (MRI)[4, 21, 22]. Traditionally, these contrast agents are simply incubated with the cells, in some cases in combination with transfecting agents, so that they are internalized primarily by endocytic uptake. Despite its simplicity and widespread use, several disadvantages are connected to this way of labelling cells. First, as endocytosis is a highly cell-type dependent process, the labelling procedure needs to be optimized for each particular nanomaterial-cell type combination. In addition, several cell types such as T-cells have difficulties in internalizing extracellular compounds through endocytosis[23]. In other cases, problems may arise for cells that have a limited life span in culture, such as pancreatic islets, as efficient cell labelling through endocytic uptake is a rather slow process[24]. A second problem is that entrapment of contrast agents in the acidic endolysosomes may lead to increased cytotoxicity, for instance by creating reactive groups on the NP surface or by leaching of toxic metal ions, such as Cd^{2+} in case of QDs[25-27]. A third disadvantage of endocytic cell labelling is that the vast majority of the contrast agents are

trafficked to the endolysosomes where they are exposed to an acidic and overall degrading environment[26, 28]. This can lead to degradation of the contrast agent, lowering the signal intensity, as reported for fluorescent labels[28-30] as well as MRI contrast agents[31-33]. In addition, it has been reported that nanomaterials trapped in endolysosomal vesicles are not distributed equally over daughter cells upon cell division[30, 34, 35]. While this process has been proposed to be a protective mechanism where the daughter cell with the highest NP load can be sacrificed in favour of the daughter cell with the lowest NP content[29, 36], recent findings show that asymmetric inheritance of vesicles is an inherent cell-biological phenomenon[37]. For quantitative cell tracking applications asymmetric inheritance of contrast agents over daughter cells is disadvantageous as it hinders accurate quantification of cell numbers over time, apart from the fact that the brightest signals are coming from cells that are suffering from the highest cytotoxicity.

In this work, we hypothesized that direct delivery of contrast agents into the cytosol could alleviate the many difficulties related to endocytic cell labelling. Evidently, this requires a technology that is able to deliver a broad range of contrast agents across the cell membrane in a fast, efficient and non-toxic manner. Vapour nanobubble (VNB) photoporation is an interesting and relatively new method that is receiving increasing interest in recent years to deliver nanomaterials into cells[38-41]. It is based on the usage of plasmonic nanoparticles, typically gold nanoparticles (AuNP), adsorbed to the plasma membrane of cells that are illuminated with pulsed laser light. If a short laser pulse (< 10 ns) of sufficiently high intensity is absorbed by an AuNP, its temperature can rapidly increase to several hundred degrees due to efficient heat confinement[42]. If the AuNP is located in hydrated tissue, like in cell culture, the water surrounding the AuNP will evaporate. This results in the generation of an expanding VNB around the AuNP surface, with a size ranging from tens to hundreds of nm depending on the laser pulse intensity. When the thermal energy of the AuNP is consumed, the VNB violently collapses causing local damage to the surrounding tissue by high-pressure shock waves. Due to the extremely short lifetime of VNBs (<1 μs), the diffusion of heat from the AuNP into the environment is negligible so that almost all energy of the irradiated AuNP is converted to mechanical energy (expansion of the VNB). This property makes VNB photoporation an interesting

technology to mechanically perforate the cell membrane, without causing unspecific thermal damage to cells. Building forth on recent successes with the cytosolic delivery of therapeutic molecules[43-45], here we show that vapour nanobubble photoporation is a well-suited technology for cytosolic cell labelling in a fast and non-toxic manner. First, we demonstrate efficient and safe loading of fluorescent dextran and QD in different cell types by photoporation. Compared to endocytic uptake, cell loading with photoporation was 50 and 3 times more efficient for FITC-dextran (FD) and QD, respectively. Combined with reduced toxicity, this enabled extended cell visualization *in vitro* over 10 generations for FD and 3 generations for QD. This shows that old-school labelled dextrans are excellent inexpensive and bio-compatible labels for cell tracking when delivered by photoporation as compared to much more expensive and toxic QDs. We demonstrate for the first time that asymmetric inheritance of fluorescent labels can be avoided by cytosolic delivery *via* photoporation. As a result, the cell intensity polydispersity remains identical over multiple cell divisions, while it rapidly increases for endocytic loading (already factor 10 after 6 divisions). Finally, we show extended *in vivo* imaging of an insulin producing cell line (INS-1E cell line) labelled with Cy5.5-dextran by photoporation. Cells labelled by photoporation could be imaged up to two months instead of only two weeks in case of endocytic labelling.

Results

Photoporation enables efficient cytosolic delivery of contrast agents with reduced cytotoxicity.

The procedure of delivering contrast agents into the cytosol of cells by vapour nanobubble photoporation is illustrated in **Fig. 1a**. Cells are first incubated with plasmonic NPs, such as gold NPs (AuNPs), for 15-30 min. During that time the AuNP can adsorb to the cells and are internalized just below the plasma membrane by endocytic uptake (see TEM images in **Figure S1**). On average ~8 AuNPs are associated per cell as determined by confocal reflection imaging (**Figure S1** and **Supporting Movie 1**). After washing the cells to remove the unbound AuNPs, the contrast agent is added and the cells are irradiated with ns (nanosecond) pulsed laser light. When a laser pulse of sufficiently high intensity is applied, the temperature of the AuNPs

increases to several hundred degrees causing the water surrounding the AuNPs to evaporate.[46] This in turn results in the formation of vapour nanobubbles that expand and collapse, thereby inducing pores in the cell membrane and allowing the contrast agent to diffuse into the cytoplasm. In our set-up, the cells are grown in a 96-well plate and the laser beam covers a circular area of ~150 µm diameter. The laser pulses are synchronized with a programmed motorized stage to assure that each cell in the culture dish receives one or two laser pulse. Scanning of the entire well takes approximately three minutes, which is essentially limited by the laser repetition rate (20 Hz). The generation of vapour nanobubbles can be confirmed with dark field microscopy (**Figure S1c**), or in time-resolved transmitted light mode (**Figure S1b**). To confirm successful photoporation of the cell membrane, we *in-situ* recorded the cytoplasmic accumulation of the cell impermeable dye Propidium Iodide (PI) (**Supporting Movie 2**, Supporting Information). To assess the size of VNB induced membrane pores, we measured the delivery efficiency of FITC-dextran of 10 kDa (FD10), 150 kDa (FD150) and 500 kDa (FD500), which have a hydrodynamic diameter of respectively 4, 17 and 31 nm. The photoporation procedure was carried out at 3 different laser fluence settings (1, 2 and 4 J/cm²). It is expected that bigger VNB are formed with higher laser fluences, which should result in bigger membrane pores as well. The data in **Figure S2a** and **S2b** show that all three probes could be delivered into 80-95% of the cells although the amount per cell is clearly less for the bigger probes. By increasing the laser fluence a slight increase in delivery efficiency was observed, indicative of slightly bigger pores. Based on FD500 delivery we conclude that pores created under the illumination conditions used in this study can have a size of at least 30 nm diameter. We also tried to estimate the pore lifetime by adding the FITC-dextran probes as a function of time after photoporation to the cells. The data in **Figure S2c and S2d** show that already after 1 min most of the cells have been completely resealed considering that only about 25% still show uptake of the smallest probe (FD10). And even in those cells the remaining pores must have been very small since the amount of FD10 taken up in those cells is about 100 fold less as when the probe is present during photoporation. Looking at FD500, there is no more uptake after 1 min, showing that all pores have become smaller than 30 nm after 1 min. After 3 min there is no further influx of any of the probes, indicating that all pores are resealed in less than 3 min after photoporation.

Since both organic probes and inorganic NPs receive much attention for long-term cell tracking, we selected FITC-dextran (FD) and CdSe/ZnS core/shell quantum dot (CdSe QD) as exemplary contrast agents. For both labels we performed a systematic comparison between endocytic labelling and cytosolic delivery by photoporation in HeLa cells in terms of uptake efficiency and cell viability. Endocytic labelling was performed by incubating the cells for 1 h with increasing concentrations of the contrast agent. Note that a 1 h incubation time was selected since QD induced toxicity became too high for longer incubation times (**Figure S3**). Photoporation was performed with a fixed concentration of contrast agents (2 mg/ml for FD and 1 µM for CdSe QD), but with increasing laser fluence settings (all above the vapour nanobubble generation threshold of ~1 J/cm^2)[43]. From the confocal images in **Fig. 1b** (END for endocytic labelling, VNB for vapour nanobubble photoporation labelling) the difference in intracellular labelling pattern is immediately clear. As expected, endocytic labelling results in a punctuate pattern due to endosomal sequestration of the contrast agent, while a uniform cytosolic labelling is obtained by photoporation. Image quantification (upper panels in **Fig. 1c**, **d**) shows that endocytic labelling results in nearly 100% of the cells with a detectable signal. For photoporation approximately 80% of the cells have a detectable signal at the lowest laser fluence of 1 J/cm^2, which becomes >90% for higher fluences. The difference in efficiency between both labelling methods, however, becomes apparent when looking at the total signal per cell, expressed as the relative mean fluorescence intensity rMFI (rMFI = MFI labelled cells / MFI control cells) (middle panel in **Fig. 1c, d**). For instance, at a laser fluence of 4 J/cm^2, cells labelled with FD by photoporation are as much as 50 times brighter as compared to endocytic labelling at the highest concentration tested. While the difference was less pronounced in case of CdSe QD, still a 3 times higher labelling intensity was found in case of photoporation. In terms of cytotoxicity (lower panels in **Fig. 1c, d**), endocytic uptake of FD did not have any effect on the cells. For photoporation the cell viability was close to 90% regardless of the laser fluence used. Endocytic uptake of CdSe QD resulted in a concentration dependent cytotoxicity. Only for the lowest concentration (100 nM) >80% cell viability was obtained. A similar concentration dependent toxicity was found for VNB photoporation with CdSe QD. 80% cell viability was obtained at an intermediate laser fluence of 2 J/cm^2. Notably, the signal per cell for this

condition is 5 times higher as compared to endocytic labelling at the non-toxic concentration of 100 nM. Similar experiments were carried out for INS-1E cells, which is a type insulin producing cell under investigation for the treatment of type I diabetes[5]. As can be seen from the results in **Figure S4**, the findings on HeLa cells could be confirmed for INS-1E cells, indicating that the results are independent of the cell type.

Cell labelling by photoporation enables extended cell tracking *in vitro*.

So far we have shown that photoporation allows a much higher amount of label to be delivered into (the cytoplasm of) cells. Combined with the fact that endolysosomal degradation or quenching of the label is avoided when contrast agents are directly delivered to the cytoplasm, we hypothesized that those cells can be imaged over an extended number of cell generations as compared to cells labelled by endocytosis. In the following experiments, a laser fluence of 2 J/cm^2 was used, for which the cell viability remains above 80% for both FD and CdSe QD (cfr. **Fig. 1c, d**). Following photoporation with the FD or CdSe QD, we monitored the mean fluorescence intensity (MFI) of the labelled cells over multiple generations by flow cytometry. The data in **Fig. 2a** and **b** show the decrease in cell intensity over time relative to the MFI at t = 0 (i.e. immediately after labelling). The signal decrease for the photoporated cells (**Fig. 2a, b**) is solely due to dilution of the contrast agent upon subsequent cell divisions. Indeed, with a mono-exponential fit we obtained a cell division time of ~25 h for HeLa cells, which is in perfect agreement with reported values[47]. To corroborate this finding, a similar test was performed on faster (C17.2 cells) and slower (INS-1E cells) dividing cell lines, resulting in the expected doubling times of ~17 and ~39 h, respectively (**Figure S5**). Importantly, a signal decrease that is only attributed to dilution by cell division is the best one can achieve for extrinsic contrast agents. Instead, cells labelled by endocytosis exhibited a much more rapid decrease of the cell signal (**Fig. 2a, b**), due to other processes than cell division alone, most importantly label degradation (CdSe QD) or fluorescence quenching (FD) in the acidic endolysosomes[26, 28].

To more precisely quantify the gain in long-term cell visibility of photoporated cells, we determined the percentage of detectable cells, i.e. cell with an intensity higher than unlabelled control cells, over multiple

cell generations by flow cytometry (**Fig. 2c, d**). Although both delivery methods resulted in more than 90% positive cells immediately after cell loading, the number of detectable cells quickly decreased in case of endocytic labelling for both FD and CdSe QD. Already after one cell division 20% of FD labelled cells became undetectable, and after 5 cell divisions the cells could no longer be detected. Instead, when cells were loaded with FD by photoporation, nearly 100% of the cells remained visible for 5 generations. Even after 7 divisions more than 80% of these cells were still detectable. Similar results were found for CdSe QD loaded cells. After one cell division only ~30% of cells labelled by endocytosis could be detected, while this was still >90% for photoporated cells. After three cell divisions >70% of photoporated cells could still be detected, while this was <10% for endocytic labelling. The main reason why FD labelled cells can be detected for much longer time as compared to CdSe QD labelled cells is due to a higher loading efficiency of FD by photoporation (cfr. **Fig. 1c, d**).

Similar experiments were performed with the INS-1E cell line (**Figure S6**). For FD labelled cells the results were identical to those obtained in HeLa cells. For CdSe QD labelled cells the difference between labelling by endocytosis and photoporation were even more pronounced. Almost no cells could be detected after one generation in case of endocytic loading, likely due to the long residence time in the degradative endolysosomes of the slow division rate. Instead, when CdSe QDs were delivered into the cytosol by photoporation, it was only after eight cell divisions that the signal was lost. Taken together, we conclude that delivering labels into the cytosol by photoporation significantly enhances the long-term cell visibility, with a signal decay that is solely determined by cell division. Due to the high loading capacity we find that old-school FDs clearly outperform CdSe QDs for this purpose.

Cytosolic delivery of contrast agents avoids asymmetric inheritance over daughter cells and the concomitant increase in cell labelling polydispersity.

It is known that contrast agents residing in endocytic vesicles are partitioned unequally between daughter cells during cell division[30, 37]. This results in an increasingly heterogeneous population of labelled cells with each cell division, which confounds quantification of cell numbers in *in vivo* applications. We hypothesized

that this drawback can be countered by directly delivering contrast agents into the cell cytoplasm. For a quantitative comparison between endocytosis and photoporation, we selected Alexa fluro@488 labelled dextran (AD) and InP/ZnS core/shell quantum dots (InP QD) which should be less affected by the acidic and degradative environment of the endolysosomes. This is confirmed by **Figure S7** showing that the signal decay over cell generations is only due to cell division after endocytic uptake. Hence, changes in cell intensity are only due to cell division, as is required for these experiments.

In first instance, the mitotic partitioning of the intracellular fluorescent labels in individual HeLa cells was imaged by fluorescence microscopy for two subsequent cell divisions, with pictures being taken every hour. Representative images in **Fig. 3a, b** (also see **Supporting Movie 3-6**) show that the fluorescent labels are diluted upon each imaged cell division. The punctate pattern observed in the cells labelled by endocytosis (END, left panels in **Fig. 3a, b**) is in stark contrast with the homogenous labelling of the entire cell cytoplasm in photoporated cells (VNB, right panels in **Fig. 3a, b**). However, one can still notice a slight punctuate pattern on top of the homogeneous cytosolic labelling after photoporation (see **Supporting Movie 4 and 6**). This is due to a small amount of label endocytosed during the three minutes laser treatment, as confirmed by control experiments where cells were incubated for the three minute with AD and InP QD (**Figure S8**). After two cell divisions the asymmetric partitioning of endocytosed contrast agents over daughter cells can already be noticed on sight (compare for instance D_{11} with D_{12} in **Fig. 3b**).

To more precisely quantify and characterize the mitotic inheritance of contrast agents in daughter cells, we calculated the fluorescence intensity (FI) for 155-210 mother cells and their respective daughter cells. The FI of the brightest daughter cell is plotted in **Fig. 3c** and **d** against the FI of the mother cell. In case of symmetric division, one expects each daughter cell to contain 50% of the original fluorescence. This is exactly what is observed for the photoporated cells, whose data show a slope of 0.515 for AD and 0.509 for InP QD respectively. In contrast, for cells labelled by endocytosis, the slope is 0.619 for AD and 0.605 for InP QD, implying that one of the daughter cells receives ~60% of the contrast agents (while the other receives ~40%).

To confirm these results, we went on to investigate statistically the inheritance of contrast agents by daughter cells using flow cytometry. The FI was measured immediately after labelling and after one cell division (respectively the grey and black lines in **Fig. 3e-f**). To interpret these results, we developed a statistical model describing the inheritance of materials over daughter cells. The model was applied to the experimental data to obtain the distribution that best matches the observed daughter distribution starting from the mother distribution. The result of the fitting is a parameter *p* that expresses the extent of asymmetry, with 0.5 indicating perfect symmetry. As expected from the microscopy data and in accordance with our hypothesis, for photoporated cells a *p* value of 0.50 and 0.51 was found for AD and InP QD, respectively. This result is independent of the cell type as the same observation was made in a second cell line (C17.2 cells, **Figure S9**). On the contrary, an unequal distribution of endocytosed contrast agents could be confirmed with *p* values of 0.66 for AD and 0.63 for the InP QD.

While an asymmetric division of 40/60 may not seem substantial in the first generation, it does introduce tremendous polydispersity in cell intensity over multiple cell divisions. This can be seen in **Fig. 4** where the FI distributions are shown over multiple generations for endocytic labelling (**Fig. 4a**) and labelling by photoporation (**Fig. 4b**). The polydispersity is plotted as a function of cell generation in **Fig. 4c**, clearly showing that it remains unchanged for cytosolic delivery but increases rapidly for endocytic uptake. Additionally, we applied the statistical inheritance model to the mother distributions (p = 0.51 for photoporation and p = 0.64 for endocytosis) and found that it accurately predicts the observed polydispersity trend.

Cell labelling by photoporation enables prolonged *in vivo* cell imaging.

Cell transplantation has been proposed as an attractive therapy in a multitude of pathologies. One example is type I diabetes, where insulin producing cells transplantation is a promising strategy to replenish insulin production[48]. In order to visualize whether the transplanted cells reach and remain at their target site, appropriate labelling techniques are required that enable long-term cell tracking. To confirm if the *in vitro* benefits of cell labelling by photoporation are valid *in vivo*, we labelled INS-1E cells with Cy5.5-dextrans

and InP/ZnS QD (@690nm) by photoporation and endocytosis. 1 million INS-1E cells were subcutaneously injected in the hind limbs of seven to nine weeks old Swiss Nude mice (left side: unlabelled control cells, right side: labelled cells). Fluorescence and bioluminescence images of the mice were recorded up to 55 days post injection. The fluorescent signal from InP QD labelled cells could not be distinguished from the background for either labelling methods (**Figure S10**) due to the limited loading as compared to fluorescent dextrans (*vide supra*). In contrast, the fluorescent signal of Cy5.5-dextran labelled INS-1E cells could be detected immediately post transplantation (day 0) for cells labelled by both methods **(Fig. 5).** Over time, the fluorescent signal gradually decreased, which resulted in complete signal loss for the cells labelled by endocytosis at day ~15 post injection (**Fig. 5a**). Strikingly, even after 55 days post injection, vapour nanobubble photoporated cells remained clearly detectable (**Fig. 5b**). In addition, the bioluminescent signal remained present at the injection site, which shows that the cells remained alive during the experiment (**Figure S11**). No detectable bioluminescent signal was found in other parts of the mouse bodies, indicating that no substantial amounts of viable cells (> 100) migrated away from the injection site. Note that a gradually increasing signal intensity is visible in the 'upper left part' of the mouse, which is most likely coming from the spleen and may be due to Cy5.5-dextrans that have been cleared from dead or dying cells over the time course of the experiment (two months). Overall, we can conclude that cytosolic cell labelling by photoporation clearly outperforms the classical endocytosis method for long-term *in vivo* cell tracking. Due to its higher loading capacity, we furthermore find that old-school labelled dextrans are better suited for long-term cell imaging than the newer class of more expensive and often cytotoxic QDs.

Discussion

For *in vivo* imaging of transplanted cells, labelling with the desired contrast agents is classically performed *via* simple incubation and subsequent internalization by endocytosis. This means that the contrast agent will typically be sequestered in endolysosomes, which is associated with a number of potential drawbacks. Endocytic uptake is typically time-consuming, has limited loading capacity, may lead to quenching or degradation of labels with concomitant increased cytotoxicity, and results in asymmetric division over

daughter cells. In this work we hypothesized that these shortcomings could be largely alleviated by delivering contrast agents directly into the cytosol. Photoporation was chosen to this end, as it was recently shown by our group and others to be a fast, efficient and non-toxic method to deliver therapeutic agents into the cytosol of cells, independent of cell type[40, 43, 45]. Following adsorption of a small number of gold nanoparticles to the cell membrane (~8 per cell), cells receive a single ns laser pulse so as to induce transient membrane pores by the mechanical force of vapour nanobubbles. Exogenous labels that are supplied in the cell medium can then diffuse through the pores into the cytoplasm. A particular benefit of photoporation by vapour nanobubbles is that there is no net heat transfer to the cellular environment. This means that cells experience less cytotoxicity as compared to the more traditional photothermal treatment at lower laser intensities in which case small pores are induced by heating of the cell membrane[43, 49].

As a single ns pulse per cell is sufficient, the photoporation procedure is essentially limited by the laser repetition rate. The laser used in this work had a (limited) repetition rate of 20 Hz which resulted in a treatment time of 3 min for a single well of a 96 well plate. While this is already much faster than endocytic labelling, we expect that speed can be increased further in the future by at least one order of magnitude by switching to a picosecond laser with higher repetition rate[40].

As contrast agents can be distributed throughout the entire cytoplasm, photoporation allows much higher cell labelling efficiency as compared to endocytic uptake, where contrast agents are restrained to the endolysosomal compartments. For 10 kDa FITC-dextran we observed a 50-fold increase in cell loading compared to endocytosis independent of cell type. As QDs are larger (slower diffusion) and can only be supplied in a lower molar concentration (due to cost and toxicity), the difference in loading capacity was less pronounced, but photoporation was still 3 times more efficient than endocytic uptake of CdSe QD.

When analysing the fluorescence intensity of cells labelled by endocytosis over multiple generations, we noticed that the signal intensity rapidly decreased for both FITC-dextran and CdSe QD labelled cells. Sequestration in the acidic and degradative endolysosomes results in quenching of the fluorescein label (which is strongly pH dependent) and degradation of the CdSe QD[29]. Instead, when the same labels were

delivered into the cytosol by photoporation, the signal decrease over multiple cell generations was only due to dilution in the daughter cells. Again these results were cell-independent since the same observations were made for three different cell types, including therapeutically relevant insulin producing INS-1E cells. In addition, endosomal sequestration of CdSe QD resulted in noticeable concentration-dependent toxicity, which could be largely avoided when delivered in the cytosol by photoporation. This is in agreement with a recent publication where metallic NPs were found to cause cell injury when sequestered in endosomes, but not when delivered straight into the cytoplasm[50].

Nanomaterials, like QDs, present in the endolysosomes are known to be distributed unevenly over daughter cells upon cell division[30]. Here we could confirm this observation and report for the first time that it is equally true for endocytosed molecular agents like Alexa Fluor dextran. This is perhaps not so surprising in light of the recent finding that asymmetric inheritance of vesicles is a naturally occurring cellular process[37]. Indeed, asymmetric cell division appears to be a crucial biological feature that does not only provide protection against exogenous materials, but is also involved in differentiation towards various lineages[51, 52]. Here, we hypothesized that asymmetric inheritance of contrast agents could be avoided by delivering the labels directly into the cell cytoplasm. In that case the labels are homogeneously distributed throughout the cytoplasm and there is no active mechanism that the cell can use anymore (such as motor proteins in case of endosomes) to shuttle the nanomaterials preferentially to one of the daughter cells. This was confirmed with labelling by photoporation independent of label and cell type. In contrast, in case of endocytosis, labels were divided over daughter cells in a 40/60 ratio. While this may not seem like a major problem on first sight, it does pose problems for accurate quantification of cell numbers in *in vivo* imaging after multiple cell divisions. Indeed, already after 6 generations the label polydispersity will have increased 10-fold so that it becomes increasingly difficult to accurately relate the detected signal to cell numbers. Instead, equal inheritance after cytosolic loading by photoporation ensures that the polydispersity does not increase over cell generations. This means that signal quantification remains equally accurate over time in long-term cell tracking studies, which is of major importance for instance for following-up on cell therapies. To our

knowledge, this is the first time that it is shown that asymmetric inheritance of exogenous materials can be avoided by delivering labels directly into the cytosol.

Finally, we imaged INS-1E cells *in vivo* labelled by photoporation or endocytosis. Following the injection of labelled cells in seven to nine weeks old Swiss Nude mice, we found that cells labelled with Cy5.5-dextran by photoporation can be imaged up to two months. Instead, cells labelled by endocytosis completely lost their fluorescent signal after two weeks. Due to less efficient loading with InP QD, the fluorescent signal from InP QD labelled cells could not be distinguished from the background for neither labelling method. This shows that old-school fluorescent dextrans are excellent labels for cell tracking *in vivo*, especially in combination with photoporation. Taken together, we can state that we developed a highly efficient and safe method to label cells that enables straightforward long term cell tracking.

Here, photoporation was selected for the cytosolic delivery of contrast agents into live cells since it has been shown to enable efficient loading at high throughput and with low toxicity. Although it needs to be demonstrated in future research, it could be expected that similar findings on long-term visibility and symmetric inheritance in daughter cells may be obtained with other methods that enable cytosolic delivery of contrast agents. For instance, electroporation could be explored to this end, although it is typically associated with high cell death[53] and for QD it was reported to result in marked aggregation[54]. Also molecular approaches are developed to this end where contrast agents are conjugated to ligands that – hopefully – can translocate the contrast agents into the cytoplasm, either directly across the cell membrane or across endosomal membranes after endocytic uptake. Examples are CFSE (Carboxyfluorescein succinimidyl ester)[55], but also CPP (cell-penetrating peptide) conjugates[56]. Yet it is clear that such strategies require special development of conjugates for each type of label, apart from the fact that the efficiency may be very much cell-dependent. Instead, a fast and efficient method like photoporation is entirely independent of the type of label or cell type used, and we expect that this method will see quickly increasing applications for intracellular delivery in general.

Conclusions

Direct cytosolic delivery of nano-sized contrast agents by photoporation opens up exciting avenues for improved long-term quantitative *in vivo* cell tracking. Apart from much more efficient cell loading and prolonged cell visibility *in vitro* and *in vivo* as compared to endocytic labelling, we show for the first time that asymmetric inheritance of labels can be avoided by delivering the labels directly into the cytosol through photoporation. As photoporation is independent of the cell type and contrast agent used, we expect that it will be a major benefit for improved long-term cell tracking studies. While this study focused on fluorescence labels, it will be of interest to evaluate in the future cell labelling with e.g. superparamagnetic iron oxide nanoparticles or Gd-complexes for magnetic resonance imaging.

Methods

Materials. 520 (±10) nm CdSe/ZnS quantum dots and 690 (±25) nm InP/ZnS fluorescent nanocrystals coated with a thiol oligomer, surface functionalized with -COOH groups (PEG-coated QD) were purchased from Mesolight, Inc. (#CdSe/ZnS-PEG-COOH-520 and #InP/ZnS-PEG-COOH-690, Mesolight, Inc., Little Rock Arkansas, USA). 520 (+/-15) InP/ZnS nm QD, functionalized with -COOH groups, were purchased from AC Diagnostics, Inc. (#CAIPS-520-P-1, AC Diagnostics, Inc., Fayetteville, AR, USA). 70 nm cationic AuNPs were purchased from NanoPartz (#CU11-70-P30-50, Nanopartz Inc., Loveland, CO, USA). These AuNPs had a zeta potential of 30 mV as measured by dynamic light scattering (NanoSizer, Malvern, UK). FITC-dextrans (FD) with a molecular weight of 10 kDa were purchased from Sigma-Aldrich (Belgium). Alexa Fluor @488 labelled 10 kDa dextrans (AD) (#D-22910, Molecular Probes®), Propidium Iodide (#P1304MP, Molecular Probes®) and Hoechst (cell nuclei labelling, #H3570, Molecular Probes®) were obtained from Invitrogen (Belgium). Cy5.5 labelled 10 kDa dextrans (CD) were purchased from Interchim (#FP-DZ2581, France).

Cell culture. Three different cell lines were applied in this work, namely the HeLa, C17.2 and INS-1E cell line. HeLa cells were obtained from ATCC (CCL-2) and cultured in complete cell medium which consisted of DMEM/F-12 supplemented with 10% heat-inactivated foetal bovine serum (FBS), 2 mM glutamine and 100 U/mL penicillin/streptomycin. The C17.2 neural progenitor cell line was retrieved from Sigma (Belgium) and cultured in DMEM containing 10% FBS, 5% horse serum, 2mM L-Glutamine and 100 U/mL penicillin/streptomycin. Finally, the LV-transduced INS-1E cells were cultured in RPMI completed with 10% FBS, 2mM L-Glutamine, 100 U/mL penicillin/streptomycin, 1% 100mM sodium pyruvate, 0.1% 50mM 2-mercaptoethanol and 10 mM Hepes. All cells were cultured at 37°C in a humid atmosphere containing 5% CO_2. All cell culture products were obtained from Invitrogen (Belgium) unless specifically stated otherwise.

Detection of AuNPs by confocal reflectance imaging and TEM. HeLa cells were cultured as described above. Cells were incubated with AuNPs for 30 min at 37°C at a fixed concentration of ~5×10^7 particles/ml. Cells were washed to remove unbound AuNPs. For confocal imaging the plasma membrane was stained with red fluorescent CellMask (#C10046, ThermoFisher Scientific). Confocal images were acquired with a Nikon C1si confocal laser scanning microscope using a 60× oil lens with 1.4 numerical aperture. AuNP were detected by the reflected laser light and false-colored in green. For TEM imaging, cell sections were placed on carbon-coated Cu grids (200-mesh) and visualized by a JEM 1400plus transmission electron microscope (JEOL, Tokyo, Japan) operating at 60 kV.

Generation and detection of vapour nanobubble. A homemade setup, including an optical and electrical timing system, was used to generate and detect the vapour nanobubble[37]. A pulsed laser (~7 ns) tuned at a wavelength of 561 nm (Opolette™ HE 355 LD, OPOTEK Inc., Faraday Ave, CA, USA) was applied to illuminate the AuNPs in order to generate vapour nanobubbles. Under these conditions the initial AuNP temperature will be in the order of 500 K upon absorption of a single laser pulse. Here we have taken into account that only the first 0.5 ns of the laser pulse is most efficiently absorbed since after that there is efflux of heat energy to form the vapour nanobubble and the emerging nanobubble scatters (partly) the subsequently incoming light. For a more detailed theoretical framework the reader is referred to the work by Pustovalov et al.[42]. Finally, the setup has a time-response and light scattering mode to allow detection of VNB formation[43].

Cell labelling *via* endocytosis. HeLa and C17.2 cells were seeded in 96 well plates at a density of 15000 cells/well while for INS-1E cells a density of 100000 cells/well was respected. Cells were allowed to settle overnight prior to treatment. Typically, for endocytosis experiments the cells were incubated with 2 mg/ml FITC-dextrans (FD) / Alexa@488-dextran (AD) / Cy5.5-dextran (CD) or 400 nM QDs (CdSe/ZnS @ 520 nm, InP/ZnS @ 520 nm, InP/ZnS @ 690 nm) during 1 hour at 37°C. In viability experiments also 100 and 200 nM QD dispersions were included. Subsequently cells were washed once with PBS (Invitrogen, Belgium) before performing further analysis.

Cell labelling *via* vapour nanobubble photoporation. For laser treatment, the cells were seeded at the same densities as for endocytic cell loading. Here, cells were initially incubated with AuNPs during 30 min at 37°C at a fixed concentration of ~5×10^7 particles/mL for HeLa and C17.2 cells and ~1×10^8 particles/mL for the INS-1E cells. Next, the cells were washed to remove remaining free AuNPs and a 2 mg/ml dextran dispersion (FD, AD or CD), or 1 μM QD dispersion (CdSe/ZnS @ 520 nm, InP/ZnS @ 520 nm or InP/ZnS @ 690 nm) was added just prior to the laser scanning. After the laser treatment, the cells were washed once with PBS and supplied with fresh cell medium before continuing with further analysis.

Measuring fluorescence intensity (FI) by fluorescence microscopy. Cells were imaged in a stage-top cell incubator (37°C with 5% CO_2 supplied, Tokai heat) for ~ 48 hours using a swept field confocal microscope (SFC & Eclipse Ti, Nikon, Japan). Each hour, cells were imaged with a 60× oil immersion lens (CFI Plan Apo VC 60×oil, Nikon, Japan) over a large area by stitching 25 by 25 images, thus covering ~2.15 mm by ~2.15 mm with ~1500 cells. The microscope's autofocus system was used to maintain a constant focus position on the cells. ImageJ software was used to segment the cells and calculate the fluorescence of each cell. The FI of each cell was calculated as follows:

$$FI = (FI_{cell} - FI_{BG}) \times \beta \quad (1)$$

where FI_{cell} is the total fluorescence intensity of a cell as measured by ImageJ, and FI_{BG} is the total background fluorescence intensity within the area of one cell. β used to compensate for photobleaching and was defined as $\beta = \bar{I}_0/\bar{I}_i$ where $\bar{I}_0$ is the initial average fluorescence intensity and $\bar{I}_i$ is the average fluorescence intensity after *i* times of laser scanning.

Measuring mean fluorescence intensity (MFI) by flow cytometry. Following labelling with either fluorescently labelled dextrans or QD *via* endocytosis or photoporation, cells were detached by trypsin-EDTA (Invitrogen, Belgium) treatment and collected by centrifugation. Following resuspension in flow buffer (PBS supplemented with 5% FBS) the samples were measured by flow cytometry (FACS Calibur, BD, Belgium) and 10000 events were detected per sample. The cells were excited with a 488 nm laser and

fluorescence was recorded in the 530/30 channel. For a certain time t_i after labelling, the normalized $\overline{MFI}_{t_i}$ was obtained by normalizing the population MFI (MFI_{t_i}) to the MFI of cells immediately after labelling (MFI_{t_0}):

$$\overline{MFI}_{t_i} = \frac{MFI_{t_i} - MFI_{t_i}^{ctrl}}{MFI_{t_0} - MFI_{t_0}^{ctrl}} \quad (2)$$

where $MFI_{t_i}^{ctrl}$ is the MFI of untreated cells (*i.e.* correction for contribution by autofluorescence). The following mono-exponential decay model was used to obtain the cell division time τ:

$$\overline{MFI} = 2^{-(\frac{t}{\tau})} \quad (3)$$

Finally, the relative MFI of a cell population was calculated by dividing the MFI at a certain time after labelling by the MFI of untreated cells at the same time point.

Evaluation of cell viability following cell labelling. Cells were seeded and loaded according to methods described above. Subsequently, cells were washed once with PBS, fresh medium was added and cells were allowed to recover two hours before performing the MTT assay. To this end 30 µl of a 5 mg/ml 3-(4,5-dimethylthiazol-2-yl)-2,5-diphenyltetrazolium bromide (MTT, Sigma, Belgium) solution was added to each well. Following an incubation period of three hours at 37°C the MTT containing cell medium was removed and cells were lysed using dimethylsulfoxide (Sigma, Belgium). When the formazan crystals were completely dissolved, the absorbance in each well was measured at 570 and 650 nm using an Envision Xcite multilabel reader (PerkinElmer LAS, Boston, MA). NP containing cell medium was included as a control to allow correction for the possible interaction of the NPs with the assay. Additionally, we evaluated cell viability following vapour nanobubble generation without contrast agent loading. In this way we could differentiate to what extent effects on viability were stemming from the loading method. All data are expressed as the mean ± SD (n=3).

Statistical model to describe the inheritance of contrast agents over subsequent cell generations. As reported previously, the redistribution of endocytosed NPs over daughter cells can be modelled by a convolution product of the original cell distribution with a binomial partitioning probability function[30]:

$$n_{t_1}(N_1) = \sum_N n_{t_0}(N) \times T(N, N_1) \quad (4)$$

$$T(N, N_1) = (1 - f)\delta(N_1 = N) + f[binomial(N, N_1, p) + binomial(N, N - N_1, p)] \quad (5)$$

Here, T is the transfer function and includes two binomial functions, describing the probability of N_1 endo-lysosomal vesicles containing NPs being inherited by one of the daughter cells upon division of the mother cell with N vesicles. Parameter p describes the probability of endolysosomal vesicles being allocated to a specific daughter cell during division. p = 0.5 signifies 50% chance that the daughter cell will receive the vesicle, while p = 1 means that all of the vesicles will be inherited by the daughter cell. While this model was developed for describing the repartitioning of a small number of NP containing endolysosomal vesicles (typically<100), in our work we are dealing with much higher numbers (typically >10^5 particles). When the statistical samples are large enough (typically N>100), the binomial distribution can be approximated by a normal distribution. This means that the convolution probability distribution can be approximated by a normal distribution. Similarly, the fluorescence intensity distributions of daughter cells can be convoluted by the transfer function implemented with a normal probability function:

$$F(I_1) = \sum_I F_{t_0}(I) \times T(I, I_1) \quad (6)$$

Here, I is the fluorescence intensity of a mother cell and I_1 is the fluorescence intensity inherited by one of the daughter cells after cell division. The transfer function $T(I, I_1)$ can be expressed with two normal distribution functions which describe the probability that a mother cell with intensity I transfers its contrast agents over its daughter cells in a ratio $I_1/I\text{-}I_1$:

$$T(I, I_1) = (1 - f)\delta(I_1 = I - I_1) + f[N(I_1, \mu_1, \sigma) + N(I_1, \mu_2, \sigma)] \quad (7)$$

Here, *f* is the fraction of cells that have undergone mitosis and *N* is the normal distribution function.

$$N(I_1, \mu_i, \sigma) = \frac{1}{\sigma\sqrt{2\pi}} \exp\left[-\frac{(I_1 - \mu_i)^2}{2\sigma^2}\right] \quad (8)$$

The mean μ_1 and μ_2, and the standard deviation σ are defined as

$$\mu_1 = I \cdot p, \mu_2 = I \cdot (1 - p), \sigma = \sqrt{I \cdot p \cdot (1 - p)} \quad (9)$$

where *p* is the probability that a contrast agent is inherent by one particular daughter cell upon cell division and *I* is the mother cell fluorescence intensity.

***In vivo* experiments long-term cell tracking post injection in mice.** All animal experiments were executed in accordance with national and European regulations and approved by the local Animal Ethics Committee. Swiss Nude mice (7-9 weeks old, Charles River, Chatillon-sur-Chalaronne, France) received 1 million LV-transduced (fLuc expression for bioluminescence) INS-1E cells suspended in 100 µL cell culture medium subcutaneously into both the hind limbs (left side: unlabelled control cells; right side: labelled cells). During cell transplantation, animals were anesthetized with 2% isoflurane (Isoflurane ISP, Rothacher, Basel, Switzerland) in 100% oxygen, at a flow rate of 2 L/minute. For both *in vivo* bioluminescence imaging (BLI) and fluorescent imaging (FLI), the animals were anesthetized with 2% isoflurane in 100% oxygen, at a flow rate of 2 L/minute. All the images were acquired using an IVIS *in vivo* optical imaging system (PerkinElmer, Massachusetts, U.S.A). For the BLI, D-luciferin, dissolved in PBS (15 mg/mL), was injected intraperitoneally (126 mg/kg body weight) prior to the imaging sessions. Consecutive frames were acquired each minute until the maximum signal intensity was reached. For the FLI acquisition, the EPI mode was used with an excitation wavelength at 673 nm and an emission wavelength at 707 nm for Cy5.5 according to its default value set in the system software (Living Imaging, Perkin Elmer). All reported BLI and FLI images were superimposed by a grey-scale photographic image with anatomical information and a pseudocolor image with functional/optical information. The BLI/FLI signals were expressed as total photon

flux (p/s/sr) from circular region of interests (ROI) using the Living Imaging software. The FLI signals of average radiance were also quantified in the ROI by this software (Perkin Elmer). No samples or animals were excluded from the analysis. The quantification data are expressed in average radiance of FLI or BLI with the mean ± SD (n=3). The data was compared by one-way ANOVA.

Supporting Information

Supporting Information Available: Figure S1-S11 and Supporting Movie 1-6. This material is available free of charge via the Internet at http://pubs.acs.org.

Acknowledgements

Financial support by the Ghent University Special Research Fund (Centre for Nano- and Biophotonics) is acknowledged with gratitude. RX gratefully acknowledges the financial support from China Scholarship Council (CSC). KB would like to acknowledge the Research Foundation Flanders (FWO Vlaanderen). KB also acknowledges financial support from the European Research Council (ERC) under the European Union's Horizon 2020 research and innovation program (grant agreement No 648124). FJ is a doctoral fellow of the Agency for Innovation by Science and Technology in Flanders (IWT) and KR is a postdoctoral fellow of the Research Foundation-Flanders (FWO). UH and SDS acknowledges financial support by the foundation for Innovation by Science and Technology (IWT 140061 (SBO NanoCoMIT)). UH and SL acknowledge financial support by the European Commission MC ITN Betatrain (289932) and the KU Leuven program financing IMIR (PF 2010/017).

Author contributions

KB initiated the idea of using photoporation for the cytosolic delivery of contrast agents with its expected advantages and supervised this work. Its application to in vivo cell imaging and the overall experimental design was performed together with UH. RX designed and performed the majority of the in vitro experiments aided by FJ, RDR and SL. RX developed the statistical inheritance model. SL performed the in vivo experiments with input from RX and FJ. SDS, KR, AS, JD, UH and KB advised on experiments data analysis and interpretation of results. All authors were involved in the writing of the manuscript.

Competing financial interests

The authors declare no competing financial interests.

References

1. Taylor, A.; Wilson, K. M.; Murray, P.; Fernig, D. G.; Levy, R. *Chem Soc Rev* **2012,** 41, 2707-2717.
2. Brader, P.; Serganova, I.; Blasberg, R. G. *J Nucl Med* **2013,** 54, 167-172.
3. Tabar, V.; Studer, L. *Nat Rev Genet* **2014,** 15, 82-92.
4. Himmelreich, U.; Dresselaers, T. *Methods* **2009,** 48, 112-124.
5. Sherry, N. A.; Tsai, E. B.; Herold, K. C. *Diabetes* **2005,** 54, S32-S39.
6. Zou, W. P. *Nat Rev Immunol* **2006,** 6, 295-307.
7. Cao, F.; Lin, S.; Xie, X. Y.; Ray, P.; Patel, M.; Zhang, X. Z.; Drukker, M.; Dylla, S. J.; Connolly, A. J.; Chen, X. Y.; Weissman, I. L.; Gambhir, S. S.; Wu, J. C. *Circulation* **2006,** 113, 1005-1014.
8. McCracken, M. N.; Gschweng, E. H.; Nair-Gill, E.; McLaughlin, J.; Cooper, A. R.; Riedinger, M.; Cheng, D. H.; Nosala, C.; Kohn, D. B.; Witte, O. N. *P Natl Acad Sci USA* **2013,** 110, 1857-1862.
9. Bhaumik, S.; Gambhir, S. S. *P Natl Acad Sci USA* **2002,** 99, 377-382.
10. Vande Velde, G.; Himmelreich, U.; Neeman, M. *Contrast Media Mol I* **2013,** 8, 424-431.
11. Nguyen, P. K.; Riegler, J.; Wu, J. C. *Cell Stem Cell* **2014,** 14, 431-444.
12. Ransohoff, J. D.; Wu, J. C. *Curr Vasc Pharmacol* **2012,** 10, 361-373.
13. Gu, E.; Chen, W. Y.; Gu, J.; Burridge, P.; Wu, J. C. *Theranostics* **2012,** 2, 335-345.
14. Dean, K. M.; Palmer, A. E. *Nat Chem Biol* **2014,** 10, 512-523.
15. Sutton, E. J.; Henning, T. D.; Pichler, B. J.; Bremer, C.; Daldrup-Link, H. E. *Eur Radiol* **2008,** 18, 2021-2032.
16. Walter, G. C.; Phillips, R. J.; Baronowsky, E. A.; Powley, T. L. *J Neurosci Meth* **2009,** 178, 1-9.
17. Clarke, J. W., Using Fluorescent Dyes for Fate Mapping, Lineage Analysis, and Axon Tracing in the Chick Embryo. In *Molecular Embryology*, Sharpe, P.; Mason, I., Eds. Humana Press: 2009; Vol. 461, pp 351-361.
18. Wegner, K. D.; Hildebrandt, N. *Chem Soc Rev* **2015,** 44, 4792-4834.
19. Michalet, X.; Pinaud, F. F.; Bentolila, L. A.; Tsay, J. M.; Doose, S.; Li, J. J.; Sundaresan, G.; Wu, A. M.; Gambhir, S. S.; Weiss, S. *Science* **2005,** 307, 538-544.
20. Gao, X. H.; Cui, Y. Y.; Levenson, R. M.; Chung, L. W. K.; Nie, S. M. *Nat Biotechnol* **2004,** 22, 969-976.
21. Xu, C. J.; Miranda-Nieves, D.; Ankrum, J. A.; Matthiesen, M. E.; Phillips, J. A.; Roes, I.; Wojtkiewicz, G. R.; Juneja, V.; Kultima, J. R.; Zhao, W. A.; Vemula, P. K.; Lin, C. P.; Nahrendorf, M.; Karp, J. M. *Nano Lett* **2012,** 12, 4131-4139.
22. Guzman, R.; Uchida, N.; Bliss, T. M.; He, D. P.; Christopherson, K. K.; Stellwagen, D.; Capela, A.; Greve, J.; Malenka, R. C.; Moseley, M. E.; Palmer, T. D.; Steinberg, G. K. *P Natl Acad Sci USA* **2007,** 104, 10211-10216.
23. Irvine, D. J.; Swartz, M. A.; Szeto, G. L. *Nat Mater* **2013,** 12, 978-990.
24. Jirak, D.; Kriz, J.; Herynek, V.; Andersson, B.; Girman, P.; Burian, M.; Saudek, F.; Hajek, M. *Magnet Reson Med* **2004,** 52, 1228-1233.
25. Oh, E.; Liu, R.; Nel, A.; Gemill, K. B.; Bilal, M.; Cohen, Y.; Medintz, I. L. *Nat Nano* **2016,** 11, 479–486.
26. Soenen, S. J.; Montenegro, J. M.; Abdelmonem, A. M.; Manshian, B. B.; Doak, S. H.; Parak, W. J.; De Smedt, S. C.; Braeckmans, K. *Acta Biomater* **2014,** 10, 732-741.
27. Su, Y. Y.; Hu, M.; Fan, C. H.; He, Y.; Li, Q. N.; Li, W. X.; Wang, L. H.; Shen, P. P.; Huang, Q. *Biomaterials* **2010,** 31, 4829-4834.
28. Martens, T. F.; Remaut, K.; Demeester, J.; De Smedt, S. C.; Braeckmans, K. *Nano Today* **2014,** 9, 344-364.
29. Soenen, S. J.; Demeester, J.; De Smedt, S. C.; Braeckmans, K. *Biomaterials* **2012,** 33, 4882-4888.

30. Summers, H. D.; Rees, P.; Holton, M. D.; Brown, M. R.; Chappell, S. C.; Smith, P. J.; Errington, R. J. *Nat Nanotechnol* **2011,** 6, 170-174.
31. Terreno, E.; Crich, S. G.; Belfiore, S.; Biancone, L.; Cabella, C.; Esposito, G.; Manazza, A. D.; Aime, S. *Magnet Reson Med* **2006,** 55, 491-497.
32. Strijkers, G. J.; Hak, S.; Kok, M. B.; Springer, C. S.; Nicolay, K. *Magnet Reson Med* **2009,** 61, 1049-1058.
33. Gianolio, E.; Arena, F.; Strijkers, G. J.; Nicolay, K.; Hogset, A.; Aime, S. *Magnet Reson Med* **2011,** 65, 212-219.
34. Yan, Y.; Lai, Z. W.; Goode, R. J. A.; Cui, J. W.; Bacic, T.; Kamphuis, M. M. J.; Nice, E. C.; Caruso, F. *Acs Nano* **2013,** 7, 5558-5567.
35. Walczak, P.; Kedziorek, D. A.; Gilad, A. A.; Barnett, B. P.; Bulte, J. W. M. *Magnet Reson Med* **2007,** 58, 261-269.
36. Errington, R. J.; Brown, M. R.; Silvestre, O. F.; Njoh, K. L.; Chappell, S. C.; Khan, I. A.; Rees, P.; Wilks, S. P.; Smith, P. J.; Summers, H. D. *Cell Cycle* **2010,** 9, 121-130.
37. Derivery, E.; Seum, C.; Daeden, A.; Loubery, S.; Holtzer, L.; Julicher, F.; Gonzalez-Gaitan, M. *Nature* **2015,** 528, 280-+.
38. Shao, J.; Xuan, M.; Dai, L.; Si, T.; Li, J.; He, Q. *Angewandte Chemie International Edition* **2015,** 54, 12782-12787.
39. Wu, Z.; Lin, X.; Wu, Y.; Si, T.; Sun, J.; He, Q. *Acs Nano* **2014,** 8, 6097-6105.
40. Lukianova-Hleb, E. Y.; Wagner, D. S.; Brenner, M. K.; Lapotko, D. O. *Biomaterials* **2012,** 33, 5441-5450.
41. Boulais, E.; Lachaine, R.; Meunier, M. *Nano Lett* **2012,** 12, 4763-4769.
42. Pustovalov, V. K.; Smetannikov, A. S.; Zharov, V. P. *Laser Phys Lett* **2008,** 5, 775-792.
43. Xiong, R.; Raemdonck, K.; Peynshaert, K.; Lentacker, I.; De Cock, I.; Demeester, J.; De Smedt, S. C.; Skirtach, A. G.; Braeckmans, K. *Acs Nano* **2014,** 8, 6288-6296.
44. Lukianova-Hleb, E. Y.; Ren, X. Y.; Sawant, R. R.; Wu, X. W.; Torchilin, V. P.; Lapotko, D. O. *Nat Med* **2014,** 20, 778-784.
45. Baumgart, J.; Humbert, L.; Boulais, E.; Lachaine, R.; Lebrun, J. J.; Meunier, M. *Biomaterials* **2012,** 33, 2345-2350.
46. Skirtach, A. G.; Dejugnat, C.; Braun, D.; Susha, A. S.; Rogach, A. L.; Parak, W. J.; Mohwald, H.; Sukhorukov, G. B. *Nano Lett* **2005,** 5, 1371-1377.
47. Berger, S. M.; Pesold, B.; Reber, S.; Schonig, K.; Berger, A. J.; Weidenfeld, I.; Miao, J.; Berger, M. R.; Gruss, O. J.; Bartsch, D. *Nucleic Acids Res* **2010,** 38, e168.
48. Wu, Z.; Todorov, I.; Li, L.; Bading, J. R.; Li, Z.; Nair, I.; Ishiyama, K.; Colcher, D.; Conti, P. E.; Fraser, S. E.; Shively, J. E.; Kandeel, F. *Bioconjugate Chem* **2011,** 22, 1587-1594.
49. Lukianova-Hleb, E. Y.; Mutonga, M. B. G.; Lapotko, D. O. *Acs Nano* **2012,** 6, 10973-10981.
50. Guarnieri, D.; Sabella, S.; Muscetti, O.; Belli, V.; Malvindi, M. A.; Fusco, S.; De Luca, E.; Pompa, P. P.; Netti, P. A. *Nanoscale* **2014,** 6, 10264-10273.
51. Knoblich, J. A. *Nat Rev Mol Cell Bio* **2010,** 11, 849-860.
52. Coumailleau, F.; Furthauer, M.; Knoblich, J. A.; Gonzalez-Gaitan, M. *Nature* **2009,** 458, 1051-1055.
53. Rubinsky, B.; Onik, G.; Mikus, P. *Technol Cancer Res T* **2007,** 6, 37-48.
54. Derfus, A. M.; Chan, W. C. W.; Bhatia, S. N. *Adv Mater* **2004,** 16, 961-+.
55. Hawkins, E. D.; Hommel, M.; Turner, M. L.; Battye, F. L.; Markham, J. F.; Hodgkin, P. D. *Nat Protoc* **2007,** 2, 2057-2067.
56. Erazo-Oliveras, A.; Najjar, K.; La Dayani, L.; Wang, T. Y.; Johnson, G. A.; Pellois, J. P. *Nat Methods* **2014,** 11, 861-867.

Figure legends

Figure 1. Cell labelling by photoporation *vs.* endocytic uptake of contrast agents. a, Schematic overview of the experimental procedure to label cells by photoporation. **b,** Confocal images show successful cell labelling with FD and CdSe QD by endocytic uptake (END) and photoporation (VNB). Control images are shown for cells incubated with FD and CdSe QD, which received laser treatment without AuNPs and VNB formation. This shows that photoporation is not induced by the laser irradiation alone. **c-d**, Quantification of the percentage of positive cells (yellow), the labelling intensity per cell (cyan) and cell viability (magenta) as a function of label concentration in case of endocytic labelling and as a function of laser fluence from 1 to 4 J/cm^2 for photoporation. The cell viability is also shown for cells treated with photoporation but without addition of contrast agents, showing that the photoporation procedure in itself induces very little toxicity. (n=3)

Figure 2. Long-term visibility of HeLa cells labelled by photoporation *vs.* endocytic labelling. a-b, The normalized MFI is shown in function of time after labelling for cells loaded with FD (**a**) and CdSe QD (**b**) *via* both photoporation (VNB, orange squares in **a** and **b**) and endocytic labelling (END, black circles in **a** and **b**). Each data point belongs to one of three independent biological repeats; each data point is the average of three technical repeats. A mono-exponential decay function was fitted to the photoporation data to calculate the mean cell division time (orange lines in **a** and **b**). **c-d**, The percentage of detectable cells is shown over several cell generations for respectively FD (**c**) and CdSe QD (**d**) labelled cells. Endocytic labelling (END, grey bars in **c** and **d**) is compared with cell labelling *via* photoporation (VNB, orange bars in **c** and **d**). (n=3)

Figure 3. Inheritance of contrast agents in cells labelled by endocytosis or photoporation. a-b, Representative confocal time-lapse images show the redistribution of contrast agents (AD and InP QD) over daughter cells after two subsequent cell divisions. Endocytosed contrast agents are located inside endosomes (punctuate pattern) and are unequally partitioned over daughter cells, e.g. compare D_{11} and D_{12} of InP QD labelled cells (END, left panels in **a** and **b**). Photoporation results in uniform cytoplasmic labelling and equal distribution of the contrast agents over daughter cells (VNB, right panels in **a** and **b**). **c-d,** Based on image quantification of confocal time lapse images, the fluorescence intensity (FI) of mother cells (n=210 for AD-END, n=205 for AD-VNB, n=172 for InP QD-END, n=155 for InP QD-VNB) is plotted against the FI of their brightest daughter cell. Linear regression shows a slope of ~0.5 for photoporated cells (equal redistribution) and ~0.6 for cells labelled by endocytosis (unequal redistribution). **e-f,** Flow cytometry was used to quantify the FI of cells immediately after labelling (grey line) and after one cell division (black line). A statistical inheritance model was fitted to the data (orange line) confirming equal inheritance (p = 0.50-0.51) in case of photoporated cells (VNB, right panels in **e** and **f**) as opposed to cells labelled by endocytosis (p = 0.63-0.66) (END, left panels in **e** and **f**).

Figure 4. Asymmetric inheritance, leading to highly heterogeneous cell labelling over multiple generations, can be avoided by photoporation. a-b, Distributions of the cell fluorescence intensity (FI) is shown over multiple cell generations (G0-G7) for cells labelled with AD by endocytosis (END) (**a**) and photoporation (VNB) (**b**). As for endocytosis the intensity is close to the background after 3 divisions, the statistical inheritance model was applied (p = 0.64) to the mother distribution (G0) to simulate the distributions for G4 and G7 (dashed lines). **c**, The polydispersity $PDI = (\sigma/\bar{I})^2$ of the distributions remains the same in case of cells labelled by photoporation, while it rapidly increases in case of endocytic labelling. The data is well predicted by the statistical inheritance model with p = 0.64 for endocytosis and p = 0.51 for photoporation.

Figure 5. Long term *in vivo* imaging of transplanted INS-1E cells labelled by either photoporation or endocytosis. INS-1E cells were labelled with Cy5.5-dextran (CD) by (**a**) endocytic uptake (END) or (**b**) photoporation (VNB). Labelled cells were subcutaneously injected right hind limb of Swiss Nude mice. Unlabelled control cells were injected at left side. For three independent repeats, the fluorescence was quantified over time of labelled (orange) and unlabelled (green) cells in the indicated regions of interest (ROI). Photoporated cells were still clearly visible after 55 days, as opposed to cells labelled by endocytosis which disappeared already after 15 days.

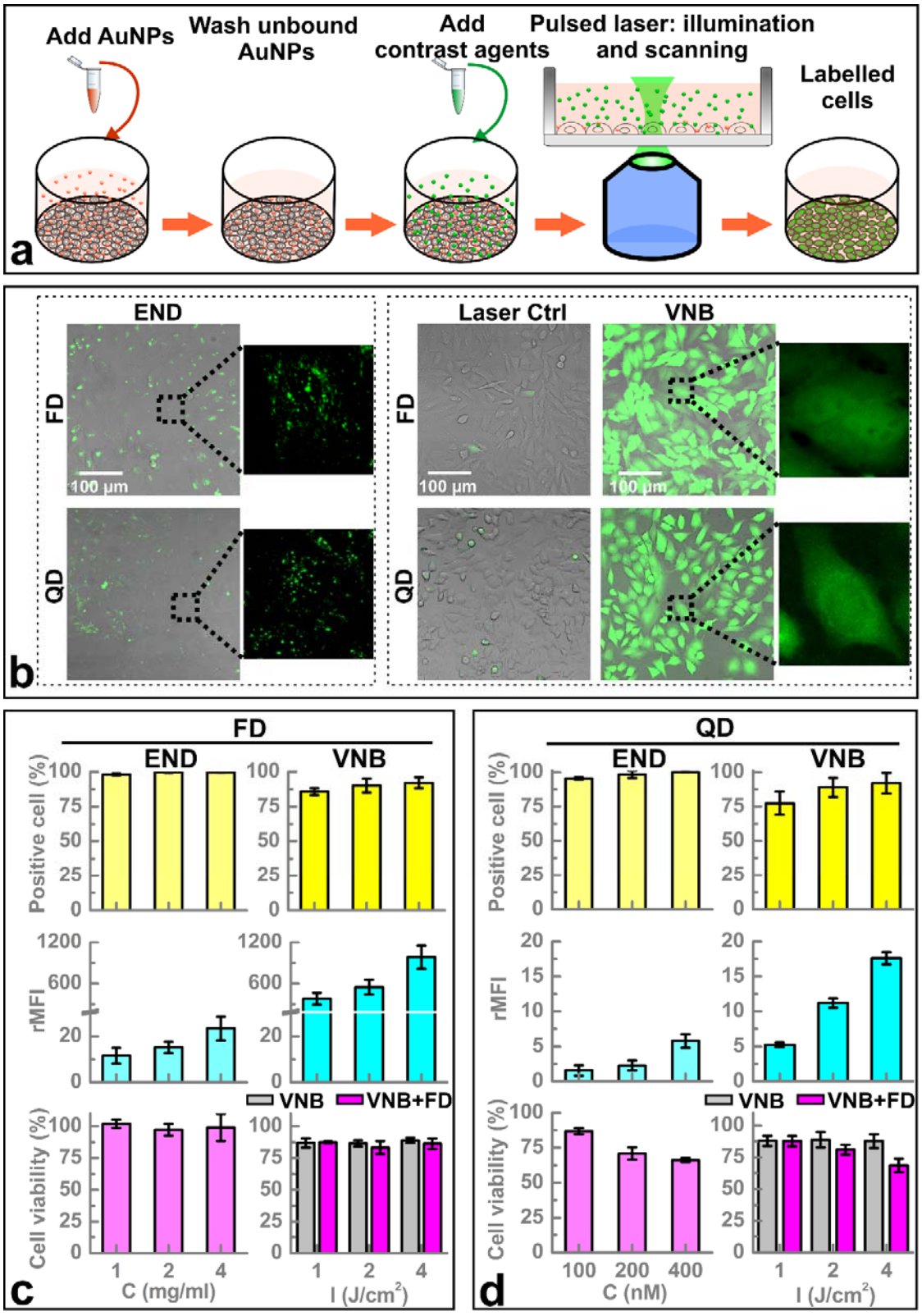
Add AuNPs
Wash unbound AuNPs
Add contrast agents
Pulsed laser: illumination and scanning
Labelled cells
a
END
Laser Ctrl
VNB
FD
QD
100 μm
b
FD
QD
END
VNB
Positive cell (%)
rMFI
Cell viability (%)
VNB
VNB+FD
C (mg/ml)
I (J/cm²)
C (nM)
c
d

Figure 1

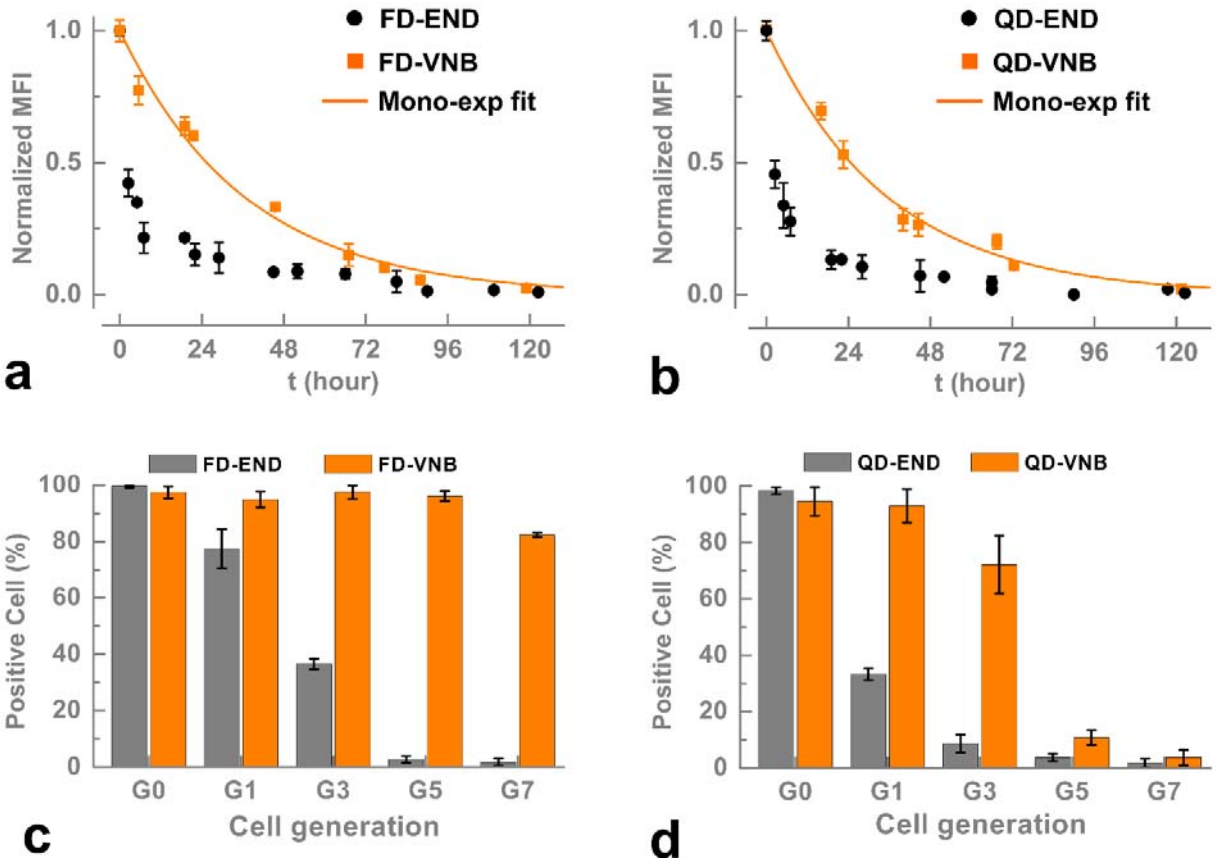
FD-END
FD-VNB
Mono-exp fit
Normalized MFI
1.0
0.5
0.0
0
24
48
72
96
120
t (hour)
a
QD-END
QD-VNB
Mono-exp fit
Normalized MFI
1.0
0.5
0.0
0
24
48
72
96
120
t (hour)
b
FD-END
FD-VNB
Positive Cell (%)
100
80
60
40
20
0
G0
G1
G3
G5
G7
Cell generation
c
QD-END
QD-VNB
Positive Cell (%)
100
80
60
40
20
0
G0
G1
G3
G5
G7
Cell generation
d

Figure 2

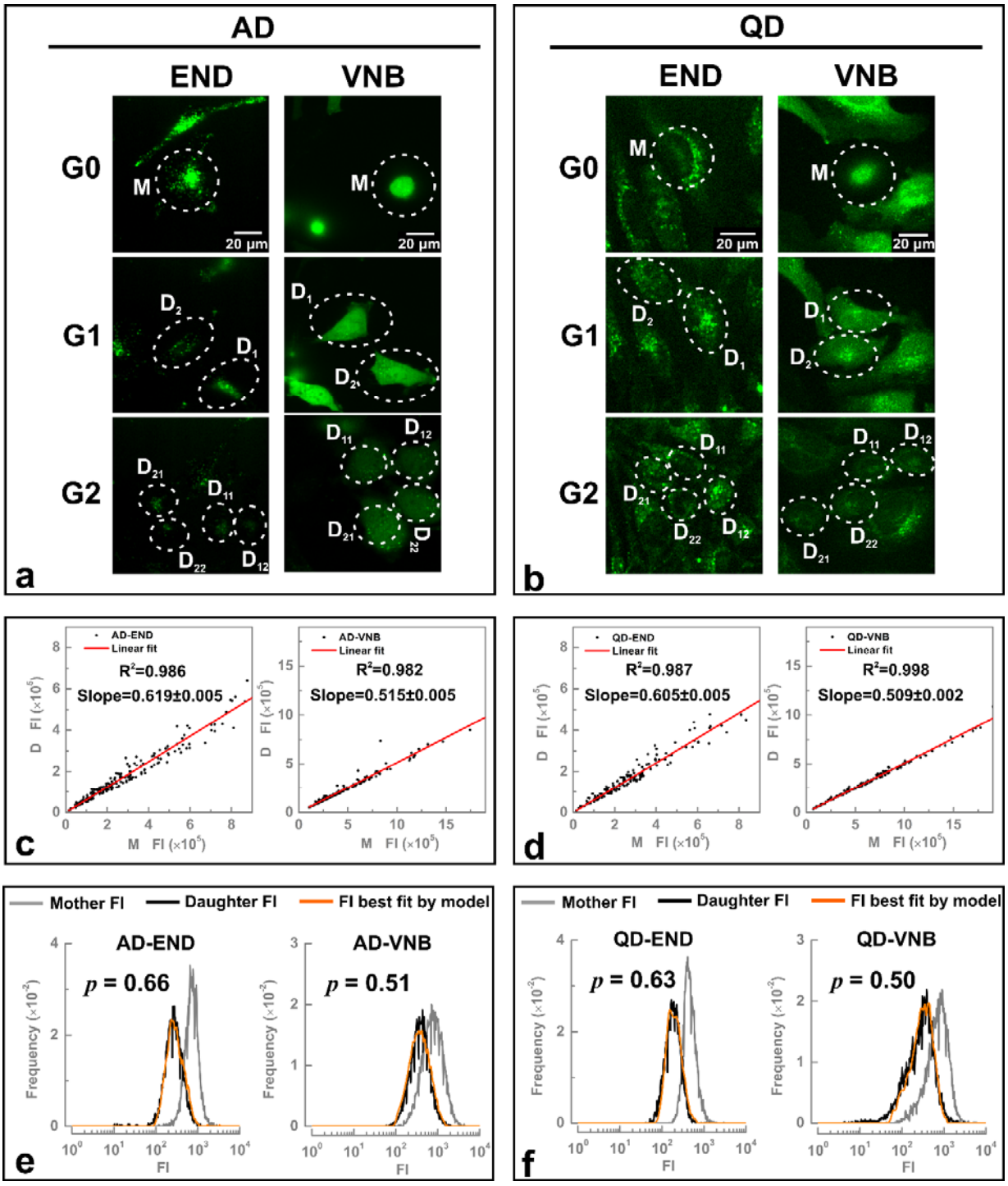
AD
END
VNB
G0
G1
G2
M
D2
D1
D21
D11
D22
D12
20 μm
a
QD
b
AD-END
Linear fit
R²=0.986
Slope=0.619±0.005
AD-VNB
R²=0.982
Slope=0.515±0.005
D FI (×10⁵)
M FI (×10⁵)
c
QD-END
R²=0.987
Slope=0.605±0.005
QD-VNB
R²=0.998
Slope=0.509±0.002
d
Mother FI
Daughter FI
FI best fit by model
AD-END
p = 0.66
AD-VNB
p = 0.51
Frequency (×10⁻²)
FI
e
QD-END
p = 0.63
QD-VNB
p = 0.50
f

Figure 3

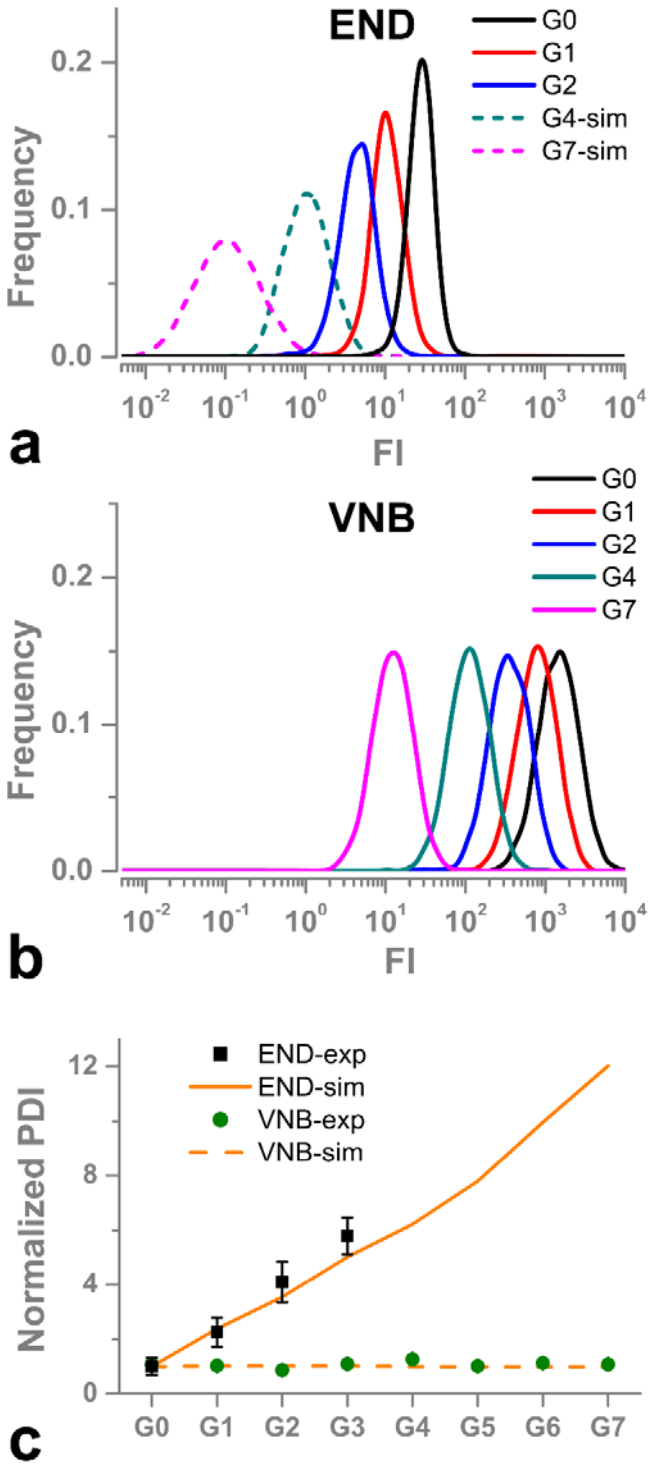
END
G0
G1
G2
G4-sim
G7-sim
Frequency
0.2
0.1
0.0
10^-2 10^-1 10^0 10^1 10^2 10^3 10^4
FI
a
VNB
G0
G1
G2
G4
G7
Frequency
0.2
0.1
0.0
10^-2 10^-1 10^0 10^1 10^2 10^3 10^4
FI
b
END-exp
END-sim
VNB-exp
VNB-sim
Normalized PDI
12
8
4
0
G0 G1 G2 G3 G4 G5 G6 G7
c

Figure 4

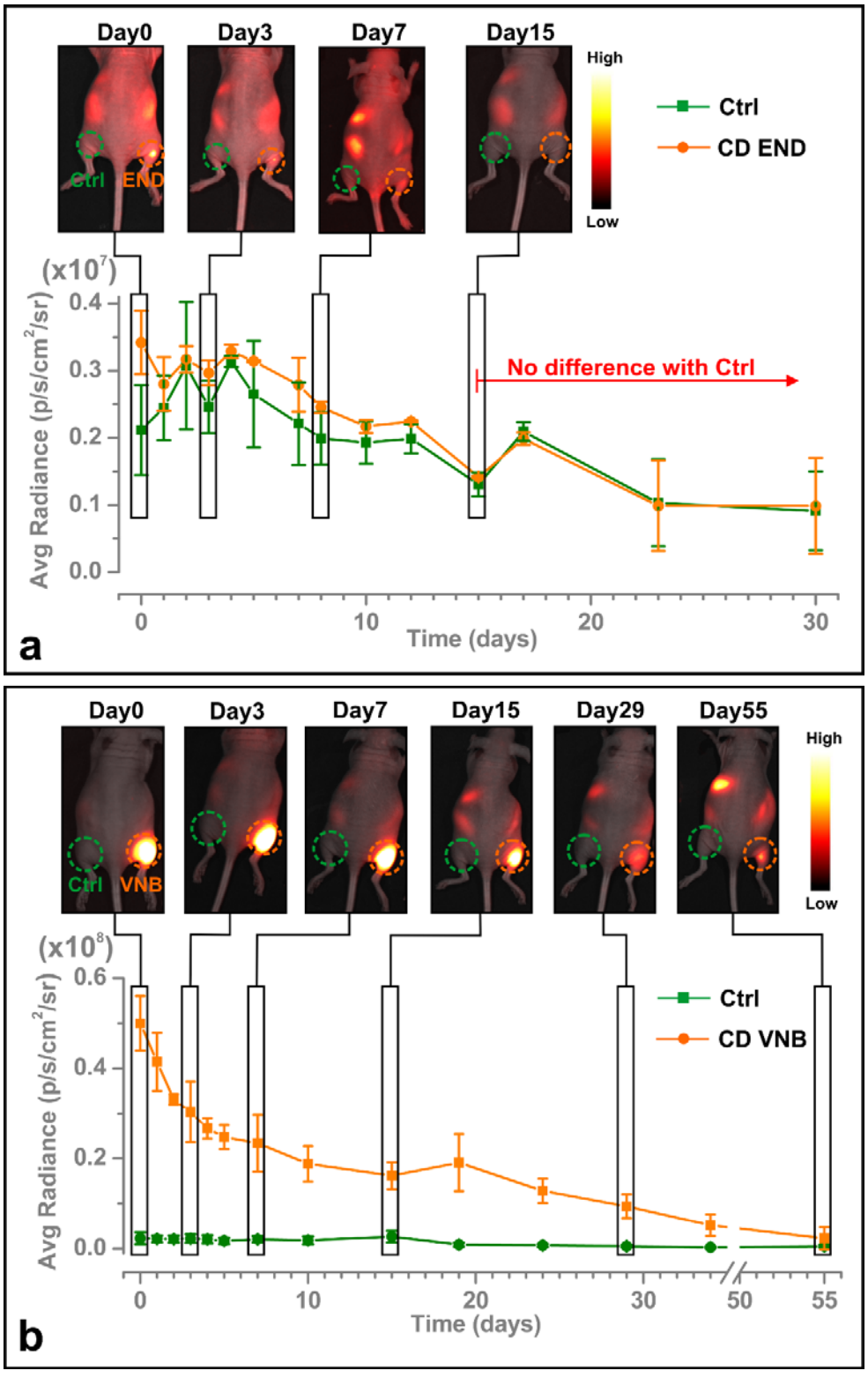
Day0
Day3
Day7
Day15
Day29
Day55
High
Low
Ctrl
END
VNB
Ctrl
CD END
CD VNB
No difference with Ctrl
(x10^7)
(x10^8)
Avg Radiance (p/s/cm^2/sr)
Time (days)
a
b

Figure 5